LAWRENCE
LIVERMORE
NATIONAL
LABORATORY

LLNL-JRNL-407978

Water confined in nanotubes and between graphene sheets: A first principle study

G. Cicero, J. C. Grossman, E. Schwegler, F. Gygi, G. Galli

October 21, 2008

Journal of the American Chemical Society

Disclaimer

Water confined in nanotubes and between graphene sheets: a first principle study

Giancarlo Cicero[1], Jeffrey C. Grossman[2], Eric Schwegler[3], Francois Gygi[4] and Giulia Galli[4]*

[1] Politecnico of Torino, Torino, Italy.

[2] Center of Integrated Nanomechanical Systems, University of California, Berkeley.

[3] LLNL, Livermore, CA.

[4] University of California, Davis, CA

Corresponding Author: G. Cicero, e-mail: giancarlo.cicero@polito.it

TITLE RUNNING HEAD. Water in hydrophobic confinement

ABSTRACT. Water confined at the nanoscale has been the focus of numerous experimental and theoretical investigations in recent years, yet there is no consensus on such basic properties as diffusion and the nature of hydrogen bonding (HB) under confinement. Unraveling these properties is important to understand fluid flow and transport at the nanoscale, and to shed light on the solvation of biomolecules. Here we report on a first principle, computational study focusing on water confined between prototypical non polar substrates, i.e. single wall carbon nanotubes and graphene sheets, 1 to

[*] Physics Department, Politecnico of Torino, C.so Duca degli Abruzzi 24, 10129 Torino, Italy. Tel. +39 011 5647370, Fax. +39 011 5647399, E-mail: giancarlo.cicero@polito.it

2.5 nm apart. The results of our molecular dynamics simulations show the presence of a thin, interfacial liquid layer (~ 5 Å) whose microscopic structure and thickness are independent of the distance between confining layers. The properties of the hydrogen bonded network are very similar to those of the bulk outside the interfacial region, even in the case of strong confinement. Our findings indicate that the perturbation induced by the presence of confining media is extremely local in liquid water, and we propose that many of the effects attributed to novel phases under confinement are determined by subtle electronic structure rearrangements occurring at the interface with the confining medium.

I. INTRODUCTION

Water confined in nanometer-sized channels or pores is expected to have structural and dynamical properties different from those of the bulk liquid[1-8]. In recent years a widespread effort has been dedicated to understand how the properties of water change upon nanoscale confinement and how these changes may influence a wide range of systems, e.g. biological systems, flow in organic and inorganic media, the properties of materials such as zeolites and cements, and nanoparticles in solution. An important question concerns the influence of the confining medium, in particular whether a confined phase of water exists that is independent of confining surfaces or whether interface properties represent the dominant influence on the nanoscale liquid. In the absence of confinement, many experimental results (see e.g. Ref 9-11) indicate that the perturbation of water at both hydrophilic and hydrophobic interfaces is local, however it is yet unclear whether such locality of the perturbation persists at the nanoscale. In addition, results on the diffusion properties of the confined liquid are rather controversial.

Several years ago fast transport of water in carbon nanotubes (CNT) was reported by Hummer *et al*.[1] who, using classical molecular dynamics (MD) simulations, found that for small diameter tubes (8.1 Å) diffusion occurs through a burst-like mechanism, stemming from the presence of single file water chains capable of moving with little resistance. These results were later rationalized with a simple coarse-grained model of a nanotube immersed in water[2] and similar findings were reported for model biological pores[3]. Exceptionally fast mass transport in CNT was also found by Holt *et al*.[4] and by

Majumder *et al*.[5] in very recent experiments, which were however conducted for tubes of larger diameter than those studied in Ref. 1-3 (~ 2nm and ~ 7 nm in Ref. 4 and 5, respectively). The TEM measurements of Naguib *et al*.[12] on water embedded in ultra thin CNT, indicated instead that the fluid mobility is greatly decreased. Similar conclusions, but for different confining surfaces, were reached by Major *et al*.[13] who observed a dramatic change in the mechanical properties of water at the nanometer scale. For confining hydrophilic surfaces with separation less than 1 nm, the viscosity of the fluid measured in Ref. 13 was 7 orders of magnitude greater than that of the bulk at room temperature. In contrast, studies of the viscosity of water confined between mica surfaces[14-15] (at distances equal to or smaller than 3.5 ±1 nm) do not point at fast transport, with measured viscosity values[14-15] within a factor of three of the bulk.

Several studies[7,16-17] have shown that confined water freezes at a lower temperature[18] than the bulk liquid, and that new ice-phases appear to be stabilized by confinement. In particular, Koga *et al*.[7,16] used classical MD simulations to show that in CNTs (with diameters ranging from 1.1 to 1.4 nm) water can exhibit structural and phase transitions under an axial pressure of 50 MPa to 500 MPa. Following this work, Kolesnikov *et al*.[17] performed neutron scattering experiments on water contained in CNT and identified an ice-shell plus a water chain structure that shows soft, "fluid-like" behavior even at temperatures as low as 50 K. Monolayer and bilayer ice structures were also reported for water confined between graphene sheets by Zangi *et al*.[19-20] when pressure was applied to the system. However, results of other classical simulations showed water freezing between graphene layers at ambient temperature[21], but pressure values were not determined in this case and thus a consistent comparison with other, similar works is not straightforward.

Building on the pioneering work of Rahman and Stillinger[22], classical MD simulations have been extensively used to study the properties of bulk water and recently also of confined water; various force fields have been employed, including simple point charge models (either rigid or flexible SPC) or other parameterizations such as TIP3P and TIP4P[23]. For example, using a flexible SPC model, Martì *et al*.[24-28] studied confinement in CNT and within graphene sheets, and they observed the presence of layered

structures, that exhibit a substantial number of broken H-bonds, and a self-diffusion along the tube axis that is faster than in the bulk. On the contrary, lower mobility was reported by Mashl *et al*.[6] who, using a rigid SPC model found that at ambient conditions water in (9x9) CNT undergoes a transition to a state with ice-like mobility. Similarly, Liu *et al*.[29,30] reported axial and radial diffusivities in CNTs much lower than those of the bulk, with diffusivity decreasing with the diameter of the tube. Hanasaky *et al*.[31] also observed slower diffusion under confinement and found that the dependence of water mobility (namely, H-bond lifetime) on the tube diameter is not monotonic. Finally, Choudhury *et al*.[32] reported that both the translational and re-orientational mobilities of water confined between graphene sheets are greatly decreased for separations below 1.3 nm. We note that in Ref. 29-32 a rigid SPC model was used, at variance from Refs. 24-28 where flexible models were adopted.

The brief (and incomplete) summary presented above clearly highlights inherent difficulties still present experimentally in probing the properties of confined water, and a dependence of results on the parametrization of force-fields, in classical MD simulations. A discussion of the sensitivity of confined water properties on force fields has been given, for example, in Ref. 33 where quantum chemistry calculations were used to benchmark some classical potential results. It is therefore of interest to study confined water with simulations that do not rely on any fitted parameters, in order to investigate microscopic properties not yet accessible to experiment (e.g. interfacial microscopic structure), including electronic structure effects.

In this paper we restrict our attention to hydrophobic confinement, and we report on a theoretical study based on *first principle* MD aimed at understanding structural and diffusion properties of water confined in single wall carbon nanotubes and between graphene sheets—systems that have received much experimental attention lately. We investigated the properties of the liquid as the separation between confining surfaces (CNT radius and distance between graphene sheets) is varied, with the goal of establishing the influence of the interface on structural and diffusion properties. The presence of a surface induces density oscillations in the liquid, with a thin region from which water molecules are excluded, followed by a layer with increased particle density. The structure of the liquid within this

interfacial layer is substantially different from that of the bulk, but it does not depend on surface separation, indicating that the nature of the perturbation induced by the surface is well localized, down to very small confinement separations. The electronic and mass density averaged over the interfacial layer are smaller than those of the bulk. However, even for very small separations, the HB network of the confined liquid is found to be similar to that of the bulk, outside the thin interfacial layer (~ 5 Å). We find that lateral diffusion and re-orientational motion of water molecules become faster under confinement, possibly due to a decrease of the dipole moment of interfacial molecules and thus weaker HBs at the interface.

II. METHOD

In this work, water was confined between graphene sheets (planar confinement) and within single wall CNT (cylindrical confinement) (see Table I). The starting configurations for the *first principle* simulations were obtained by performing MD simulations (NVT) with SPC/E classical potentials[34]. We chose the SPC/E model because tested parameters to describe the interaction between water and graphite surfaces and nanotubes were available in the literature[35]. In particular the carbon atoms were modeled as neutral particles interacting with the oxygen atoms through a Lennard-Jones potential determined by the parameters $\in_{co}$ = 0.3135 kJ/mol and σ_{co} = 0.319 kJ/mol[35]. In the graphene/water system the cell dimensions in the wall plane (x,y) were fixed and determined by the size of a relaxed graphene sheet containing 60 carbon atoms (12.4 Å / 12.1 Å). Carbon-carbon distances were fully optimized. In the z direction, the interlayer separation was varied, while keeping the number of water molecules constant, until the stress along this direction yielded a pressure equal to atmospheric pressure. Three confined water systems were considered with graphene layers at 10.09, 14.41 and 25.02 Å distance. From these calculations we estimated the thickness of the exclusion volume present at the graphene/water interface to be ~ 2 Å. This thickness was employed in the case of NT confinement to determine the number of molecules needed to fill up the tubes in order to obtain a density of ~ 1 g/cm^3. We used two semiconducting tubes to confine water, namely a (19×0) NT and a (14×0) NT, which have

a diameter of 15.0 Å and 11.1 Å respectively. The length of the tube (i.e. the number of minimal unit cell in the axial direction needed to accommodate more than 30 water molecules) was 17.065 Å for the (19×0) NT and 25.251 Å for the (14×0) NT. All samples were classically equilibrated for 100 ps and the final structure was then used as input for the *first principle* simulations.

We used Density Functional Theory (DFT)[36,37], in the generalized gradient corrected approximation (PBE)[38], and Born-Oppenheimer (BO) molecular dynamics (MD). We employed non-local pseudopotentials[39], the electronic wavefunctions (charge density) were expanded in plane waves, with energy cutoff up to 85 (340) Ry and the integration over the Brillouin zone was performed with the Γ point of the supercell. The numerical integration of the ion equations of motion was carried out with a time step of 20 a.u. (8 electronic steps using preconditioned steepest descent with Anderson extrapolation were performed to obtain the electronic ground state at each atomic step). In our *first principle* calculations, the atomic configuration obtained with a classical simulation run was first equilibrated with a velocity rescaling technique for about 3 ps at 400 K. Then the thermostat was removed and statistics was collected for the simulation time reported in Table I. All the calculations were done considering D_2O instead of H_2O; this allows one to employ larger MD time step and thus to simulate for longer times with the same amount of computer resources.

Since the purpose of the present investigation was to compare the properties of confined water with those of bulk water, we considered the temperature (400 K) at which, for bulk water, DFT using PBE and BO dynamics yields results in good agreement with experiment for structural and diffusion properties at ambient conditions[40,41]. There are several possible reasons why elevated simulation temperatures are required in the *first principle* simulations. For instance, van der Waals (vdW) dispersion interactions are not expected to be accurately reproduced by semi-local GGA functionals such as PBE or BLYP. However, we note that of the three contributions to vdW forces – induction, thermal orientation and dispersion – it is the dispersion forces that are not well described, and in liquid water, their strength is approximately one order of magnitude smaller than that of hydrogen bonding. As pointed out in Refs. 41-42, in addition to possible inaccuracies in the GGA functionals, it is possible

that a large fraction of the disagreement is due to the neglect of the quantum motion of hydrogen atoms in the simulations. All DFT based molecular dynamics simulations of water (except for one[43]) have been carried out using a classical description (Newtonian dynamics) of the proton dynamics. There is growing evidence based on empirical potentials fit to quantum chemical data that proton quantum effects in water may be more pronounced than previously thought (e.g. see Ref. 41); hence it is possible that commonly used GGA functionals such as PBE and BLYP yield a quite accurate description of hydrogen bonding in water, once proton quantum effects are taken into account. We also note that approximately accounting for quantum effects via temperature rescaling is a technique that has been used in a variety of materials other than water[44,45].

At 400K, the computed diffusion coefficient of bulk water is ~ 1 10^{-5}cm^2/sec. A statistical error bar on this number can be estimated from a convergence of the diffusion coefficient as a function of simulations time, carried out for a potential yielding very similar diffusion and structural properties for the liquid. We carried out such a convergence study in Ref. [40-41], where the error of the self-diffusion constant obtained over 20 ps simulations is found to be 20-30%.

In addition to studying liquid water in contact with graphene and carbon nanotubes, we also investigated the interaction of a single water molecule with a graphene plane, by considering both the equilibrium structure at T=0 and snapshots taken from our 400K MD trajectory. While at T=0 a water molecule is found to be barely bound to graphene (with a binding energy of ~ 0.25 kcal/mole), for configurations corresponding to finite T, we find a binding energy (defined as the difference between the energies of the interacting and non interacting graphene/water system) of 1-2 kcal/mole. In the high T configurations, thermal energy induces bond distortions in the graphene sheet and in the water molecule, resulting in local dipoles (charge transfer) that strengthen water/graphene interaction. In addition, at finite T, we find overlap between the carbon and water charge densities and electron-dynamical effects that are responsible for characteristic features detected in IR spectra (these are discussed in detail elsewhere[46]). A variety of values have been reported experimentally and theoretically for the interaction of gas phase water with graphite and these are summarized in Ref. 47.

Our *first principle* MD simulations were carried out using *Qbox*[48], while maximally localized Wannier functions, used to compute water molecular dipole for selected MD configuration, were obtained by using the *GP* code[49] following the scheme proposed by Gygi *et al*.[50]. Finally, classical simulations were performed with *GROMACS*[51].

III. RESULTS AND DISCUSSION

In this section we first describe the results of our simulations, then we present an interpretation of our findings. Table I summarizes the simulations carried out in the present study.

Structural Properties--The analysis of the water density in the direction perpendicular to the surface reported in the top panels of Fig. 1 reveals density oscillations typical of a liquid in contact with a hard wall[10,52-53]. In particular, in the case of graphene we found that water molecules are excluded from a region with thickness of ~ 2.5 Å; the particle density rises sharply outside this excluded volume, with a first peak extending up to 5 Å, similar to what found for water on hydrogenated diamond surfaces[46], that are much less polarizable than graphene sheets. The height of this peak increases with decreasing distance between the surfaces (from 2.38 g/cm^3 to 1.96 g/cm^3 in going from 10.09 Å to 25.02 Å), but its position is independent of the confining length. From a comparison of the top panels of Fig. 1 (a-e) it is clear that increased confinement results in enhanced density oscillations. This may be understood in terms of interfering effects of the two facing surfaces, and at extreme confinement the perturbation induced on water at the two interfaces is amplified. In panel (c) of Fig. 1, where the distance between graphene sheets is the largest (25.02 Å), density oscillations are nearly suppressed, indicating that the effect of the surface perturbation is highly localized. In this case, only the water layer close to the surface has density higher than the bulk; beyond ~ 5 Å from the surface the density curve becomes flatter and reaches the bulk value (1.0 g/cm^3). We note that in all of the deuterium density profiles reported in Fig. 1, a small shoulder is present in the first density peak, which indicates a slight preference for some interfacial water molecules to orient with an OD bond pointing towards the surface.

The middle panels of Fig. 1 show the variation of the electronic density (ρ_{el}) in the direction

perpendicular to the surface. In the region from which water molecules are excluded, we observe a sharp decrease of ρ_{el}, which vanishes at about 2 Å. These findings are consistent with the results on the electronic density as obtained from X-ray measurements by Poyron et al.[54]. In this region the contributions to ρ_{el} come almost entirely from the surface carbon atoms. Outside this layer of zero particle density, we observe oscillations of ρ_{el}; their intensity is slightly larger at the position of the first sharp peak in the particle density distribution than in the center of the slab. Very similar results were obtained also for *first principle* simulations of water confined by hydrogentated diamond surfaces.[46]

Interesting structural information about confined water is also obtained from an analysis of the bottom panels of Fig. 1, where the average number of hydrogen bonds (HBs) per water molecule is reported as a function of the distance from the surface. Interfacial molecules, although surrounded by only half of a bulk coordination shell, are still engaged in a relatively large number of HBs. In particular in the 5 Å interfacial layer, the number of HB (2.5) amounts to about 70% of the corresponding bulk value (recovered in the middle of the slab). This observation is consistent with the experimental finding on the structure of interfacial water as obtained through vibrational spectroscopy by sum-frequency generation (see e.g. Ref. 55), it also agrees with previous molecular dynamics simulations in which it was found that water in contact with solid surfaces[52,53,56] readily restores its liquid, bulk-like hydrogen bonded network, just outside the thin interfacial layer. The thickness of this layer is slightly larger than in the hydrophilic case where, e.g. for hydroxilated Si-SiC surfaces[56], we found values of ~ 3.5 Å. The dashed and dotted curves in the bottom panels of Fig. 1 represent, respectively, the number of HB acceptors and donors of each water molecule in our samples. When approaching the confining surface, a water molecule preferentially has a higher number of HB donors; thus, most of the time, one of its deuterium atoms is not engaged in HBs, consistent with features observed in the analysis of the OD tilt angle distribution (see Fig. 2). This property appears to be independent of the confinement distance, and it is rather determined by the water/surface interaction.

Similar results for the structure of the interfacial layer and their dependence on water-surface interaction were obtained in the case of the two CNTs. However layering effects are enhanced in the

tubes, and cylindrical water shells appear, instead of flat layers (only one shell for the smaller tube and two for the larger one). For both tubes (see Table I), we found a very pronounced peak in the density of water in proximity of the walls [the height reaches 3.6 g/cm^3 in the case of the (14×0) NT and 2.6 g/cm^3 for the (19×0)]. Remarkably, for the smallest tube the water density in the center is almost zero, and molecules appear to be densely packed at the interface; therefore one might expect a decrease in diffusion of the fluid relative to the bulk. As we will see, this is not the case.

In order to further investigate water restructuring at the interface, we have studied the orientation of the OD bonds with respect to the direction perpendicular to the interface (radial direction in the case of nanotubes). In Fig. 2, we report the OD tilt angle distribution for water confined between graphene layers. The color maps represent the probability of finding, at a certain distance from the surface, an OD bond forming a specific angle (θ) with the direction perpendicular to the substrate (see inset of Fig. 2 for the definition of tilt angle): for every molecule two tilt angles are calculated, one for each OD bond. The probability has been multiplied by the value of the water density, to enhance the signal of the denser layers. At the interface, molecules have strong preferential orientations. In particular at about 2.7 Å from the surface two angles are favored: 75° and 150°. This geometric configuration corresponds to water molecules having one of the OD bonds nearly parallel to the surface and the other pointing towards it. At 3.3 Å, the opposite orientation in found with an OD pointing away from the surface (25°) and the other nearly parallel (100°) to it. At about 3 Å, there is a strong peak at 90°, indicating that most of the molecules have both OD bonds roughly parallel to the surface. In the high density layer, the planar orientation is preferred in order to maximize in-plane HBs. The most remarkable feature of the three maps reported in Fig. 2 is that the orientation of water bonds in the interfacial layer does not depend on surface separation. At a graphene distance of 10.09 Å, the system consists of only two water layers, yet these appear to be equivalent to the two interfacial layers observed for the 25.02 Å separation. A similar behaviour was found in the case of water confined in CNT when calculating the orientation of the OD bonds with respect to the radial direction. Although the preferential angles are slightly different because the surface is curved, the qualitative features of the angular distribution are

very similar, and the interfacial layer structuring appears to be independent on the confining distance (i.e. tube diameter). In the case of the smallest nanotube, water molecules arrange in one cylindrical shell, thus no water molecules show bonds oriented towards the centre of the cylinder, as hardly any H-bonds can be formed in that direction (the peak at ~25° in the angular distribution is not observed in this case). These results appear to be at variance from those of Hummer, *et al.*[1], that find a linear chain localised in the center of a smaller nanotube.

Fig. 3a shows the calculated oxygen (red) and deuterium (blue) spatial distribution functions (SDF) in a water layer within 5 Å from the surface for the case of water confined between graphene layers separated by 14.41 Å. A representative HB ring structure found in the first interfacial layer is shown in Fig. 3b. The SDFs represent the density distribution of oxygen and deuterium atomic positions; thus they reveal how water fills the space close to the surface. Deuterium and oxygen atoms are not uniformly distributed on top of the surface. Oxygen preferentially resides on top of the center of the hexagonal carbon rings (red isosurface). Some deuterium atoms tend to point towards the surface, as indicated in Fig. 1a-c. However, at variance with the case of a benzene molecule[42] in solution, the computed SDFs do not show any preference for the "dangling" H-bond to point towards the center of the carbon hexagons.

We note that the structural properties of interfacial water found in our *first principle* simulations are rather different from those obtained in the classical simulations we used to prepare the initial configurations for the first principle simulations. The water density oscillations are qualitatively similar in the two cases, but they are more pronounced in the first principle calculations. In particular, when a Lennard-Jones parameter of $\in$co = 0.3135 kJ/mol (same as in Ref. 35) is used to describe the carbon-water interaction, the first interfacial layer of water in the classical simulations is less intense than in the first principle simulations. In order to have similar peak heights as in the first principles simulations, we found that much larger $\in$co (~ 0.78 kJ/mol) are needed in the classical simulations. Subtle but important differences between the classical and first principle simulations can also be found in the spatial

arrangement of water molecules in the interfacial layer. Specifically, in the classical case we did not find a strong preference to orient OH bond towards the surface, as in the first principle simulations. More interestingly, we found that the SDFs of the interfacial layer are uniform in classical simulations and do not exhibit the peculiar structuring shown in Fig. 3.

Dynamical properties **---**We first analyze the Fourier transform of the deuterium atoms velocity autocorrelation function (Fig. 4), which is related to the vibrational spectra of our samples. Calculations of IR spectra will be reported elsewhere[46]. As shown in Fig. 4, for both graphene sheets and CNTs, a peak appears at frequencies higher than in the bulk spectrum (2600 cm^{-1}), in the region of the OD stretching mode. This signal is related to OD groups not involved in HBs; these OD bonds are likely to vibrate at a frequency higher than OD groups in a bulk environment and in early experimental work on the characterization of interfacial water their presence has been interpreted as a signal of surface hydrophobicity[55]. A similar feature in the power spectrum of confined water was observed by Martì *et al*.[26] and it was ascribed exclusively to confinement effects. In particular, it was interpreted as arising from the splitting of the symmetric and antisymmetric components of the OH stretching mode, accompanied by a shift of the stretching frequency to gas phase values (higher than in the bulk). With the aim of discerning between confinement and surface effects, we artificially cut our water samples in layers of increasing distance from the interface, and we calculated the power spectra of each layer. We found that the peak at 2600 cm^{-1} is mainly related to water molecules in close proximity with the surface, with non hydrogen-bonded OD bonds likely pointing towards the graphene layer. The water layer in the middle of the slab shows instead a power spectrum similar to that of the bulk liquid. This suggests that the peak at 2600 cm^{-1} is mainly due to a surface effect and confirms the locality of the perturbation induced by the surface on water, as observed in our structural analysis. We note that confinement enhances the high frequency power spectrum signal, as it increases the surface to volume ratio of the liquid. We believe this is the reason why the high frequency peak is more pronounced in the power spectra of CNT than in that of graphene sheets.

Another interesting region of the power spectrum of Fig. 4 is the band at low frequencies (120-800

cm^{-1}) that is usually assigned to librational modes, and thus related to inter-molecular hydrogen bonds. This band appears to undergo a red shift in the most confined samples, indicating a weakening of the HB strength in the interfacial region. However the simulation times available here do not permit quantitative conclusions on the shifts observed in the low frequency part of the spectrum. The band at 1178 cm^{-1}, related to the water molecule bending mode, is mostly unchanged in all of our samples.

In order to investigate molecular self-diffusion, we calculated the mean square displacement (MSD) of the oxygen in the direction parallel to the interface in the case of graphene and along the CNT axes. The MSD is related to the self-diffusion coefficient (D) through the Einstein relation, using the appropriate normalization factor for mono and two dimensional diffusion processes. Our results show that the lateral diffusion constant of water increases at extreme confinement. In particular, in the case of flat surfaces (graphene), diffusion increases with decreasing interlayer separation, becoming almost three times larger than that calculated for the bulk (1.0×10^{-5} cm^2/s), for a distance of 10.09 Å. This increase is significant and well outside the error bar on our diffusion constants, estimated to be 20-30% (see Method Section). In the case of CNTs, this effect appears to be enhanced, although it is not possible to establish a trend as a function of the tube radius from only two systems. At a diameter of 15.00 Å the diffusion constant reaches about 3×10^{-5} cm^2/s, which again is significantly different from that of bulk deuterated water. When decreasing the CNT radius to 11.10 Å, the diffusion constant slightly decreases, however remaining larger than the bulk value. In the case of two-dimensional confinement, for a CNT diameter smaller than an optimal value, the translational motion of water molecules may become so constrained that the diffusion constant does not increase as the radius decreases, unlike the case of graphene sheets.

Additional information on dynamical properties can be extracted from the re-orientational dynamics of the molecular dipole vector ($\boldsymbol{\mu}$), obtained from the correlation function $\Gamma = \langle \boldsymbol{\mu}(0) \cdot \boldsymbol{\mu}(t) \rangle$. The dipole vector of each molecule ($\boldsymbol{\mu}$) was calculated by assigning a charge of –2 to the oxygen atoms and charges of +1 to the deuterium atoms (geometrical dipole). This function, reported in Fig. 5, is characterized by an exponential decay (faster decay is associated with faster reorientation). Interestingly, we found that

the rotational motion of confined water molecules is faster than in the bulk phase, indicating that HBs are formed and broken at an increased rate. Indeed, H-bond lifetime calculated for the confined water samples show decay faster than bulk water, at variance with the results of Ref. 1 where HB lifetime under confinement where found to be substantially larger than in the bulk. Our results are consistent with weaker intermolecular HBs found in the interfacial regions. In particular, from Fig. 5 it appears that for both the CNTs and graphene layers separated by 14.41 Å, the relaxation time is almost identical, while it substantially decreases, becoming very close to that in the bulk, in the case of graphene at 25.02 Å. We repeated a similar analysis on the trajectories obtained with a classical potential (rigid SPC/E water model, see method section) and obtained the opposite result: water molecule reorientation appears hindered at increasing confinement. However we note that Marti, *et al*.[25] using a flexible SPC model did find an increased lateral diffusion of water under confinement, consistent with our results.

The faster dynamics obtained in our *first principle* simulations may be related to the magnitudes of the dipoles associated with the water molecules. These significantly decrease in the interfacial regions. The dipole moments were calculated using maximally localized Wannier function centers[57], by averaging over configurations extracted from our MD trajectories, and equally spaced in time. In the case of the bulk liquid the average molecular dipole moment calculated from MD trajectories is about 3.10 D. For graphene sheets and CNT, we found that the average dipole moment is always lower than in the bulk except for the 2.5 nm separation case where it has about the same value. Interestingly, the dipole significantly decreases within the interfacial layer assuming values of about 2.6-2.7 D for water molecules closer to the surface, while it is close to the bulk value in the liquid outside the interfacial regions. For the two CNT considered here the dipole moment remains lower than in the bulk in the whole confined sample, and the average dipole moment of the two confined systems is 2.87 and 2.93 D for the (14x0) and (19x0) CNT, respectively. In the case of a previously studied hydrophilic substrate (hydroxilated silicon carbide[56]) the lateral diffusion of water in the interfacial layer was substantially unmodified, with respect to the bulk, and correspondingly the average dipole moment of interfacial water molecules was very close to that of the bulk. On the other hand, in our study of water confined

between deuterated diamond surfaces[46], we observed a lateral diffusion enhanced, with respect to that found for the graphene case, and a smaller dipole moment of interfacial water molecules.

The variation of dipole moment magnitudes within the confined sample and with respect to the bulk may explain why rigid, non-polarizable classical models (e.g. SPC/E) do not predict fast molecular reorientation. The parameters of these models (like many others) are fitted to reproduce bulk liquid properties and it is thus not surprising that they do not account for the subtle interfacial rearrangement observed in our *first principle* simulations. Flexible and polarizable models may improve the description of the structural and dynamical properties of confined water, however the parameters entering the models may need fine tuning to describe how the strength of HB varies within a specific confined environment.

IV. SUMMARY AND CONCLUSIONS

The structural and dynamical properties reported in the previous section all consistently show that the perturbation of the confining surfaces on liquid water is localized within a 5 Å interfacial layer, whose thickness and microscopic structure do not depend on surface separation. The local nature of the perturbation found here is consistent with many results reported in the literature for bulk water in contact with both hydrophilic and hydrophobic surfaces and for complex surfaces, such as proteins[11].

This locality of the perturbation is also in agreement with the results of ultra fast optical Kerr spectroscopy reported by Scodinu *et al.*[58] for water confined in hydrophilic and hydrophobic nanopores. However Kim *et al.*[59] reported that for water in contact with organic monolayers, they find an interface layer extending up to 5 nm.

The interfacial layer found in our simulations is composed of a region of about 2.5 Å of zero particle density, followed by a region with particle density higher than in the bulk. Overall, the average density in the 5 Å interfacial layer is lower than in the bulk. In spite of an increased density of molecules outside the excluded volume, in proximity of the surface, water mobility is increased with respect to that

of the bulk. This appears to be related to a decrease of the molecular dipole moment and a weakening of HBs at the interface. These results are consistent with those reported in the case of water in the cavities of a hydrophobic zeolite[60], although the simulation time reported in Ref. 60 was rather short (3 ps) and an analysis of interfacial properties was not provided. The model of confined water emerging from our simulations –highly inhomogeneous, mobile interfacial layer surrounding a liquid which recovers bulk-like characteristic just outside a thin, ~ 0.5 nm, surface region-- is rather different from that proposed by Kolesnikov *et al.*[17]. However this study was conducted at much lower temperatures. These authors reported molecules frozen along the interior of a CNT wall in a four-fold coordinated square-ice pattern. These results were obtained using MD with classical potentials for CNTs very similar to the (19x0) case considered here, and they were used to interpret neutron scattering experiments. While our *first principle* MD results differ from the ones of Ref. 17, we note that our computed power spectrum is consistent with the generalized vibrational density of states obtained experimentally by the same authors, showing a blue shifted stretching band and a red shifted librational band. The structural model of confined water found here also differs from that obtained in another classical simulation by Byl *et al.*[61] The authors attribute their measured high-frequency infrared active mode to inter-ring OH groups different from those present in bulk water, and they propose the existence of a novel confined water phase with unusual HBs. According to our simulations the difference in HB between confined and bulk water mainly pertains to molecules within a thin interfacial layer and it does not stem from novel, liquid phases.

As mentioned in the Introduction, the mobility and in general the dynamics of confined water have received controversial interpretations in the literature. Recent flow experiments in CNTs with diameter of 2 nm or less reported by Holt *et al.*[4] showed enhanced flow at the nanoscale; these results are consistent with the enhanced lateral diffusion suggested by our simulations. However, the enhancement by orders of magnitude found in Ref. 4 is difficult to explain based on our finding of a moderate increase in the liquid self-diffusion coefficient, and viscosity calculations would be necessary to reach

firm conclusions on flow rates. Other experiments reported instead a slower dynamics in nanotubes. Naguib *et al*.[12] interpreted some of their TEM results on water confined in multi-wall CNTs as showing a decreased mobility of the liquid inside the tubes.

In the field of classical MD simulations, recent results obtained on mica by Leng *et al*.[62] for water dynamics are consistent with ours, while several other authors have reported a decreased mobility (e.g. Mashl *et al*.[6]) for water in nanotubes. Faster diffusion has been predicted in the case of very small nanotubes in Refs. 1-3, where one chain of water molecules was present and, for larger tube diamaters, by Martì *et al*.[25] who employed a flexible SPC model to describe confined water. When using classical potentials, water-water and water-surface interactions are not usually treated on the same footings. For example, Pertsin *et al*.[33] have shown that different water-graphite potentials may yield rather different structures in the interfacial region, although thermodynamic properties may be less affected by the presence of confining surfaces, as discussed in Ref. 63. In addition, classical potentials are usually fitted to bulk properties and they are thus unlikely to account for subtle but important effects, such as the decrease of interfacial water molecule dipole moments and electronic structure re-arrangements at the surface. Our results point at the need for at least flexible and possibly polarizable models, in order to describe water confinement effects in a realistic manner.

ACKNOWLEDGMENT

We thank D. Prendergast, T. Ogitsu and M.Sharma for many useful discussions. Part of this work was performed under the auspices of the U.S. Department of Energy by Lawrence Livermore National Laboratory under contract No. DE-AC52-07NA27344. Use of the computing facilities at the Lawrence Livermore National Laboratory (LLNL) is gratefully acknowledged.

FIGURES

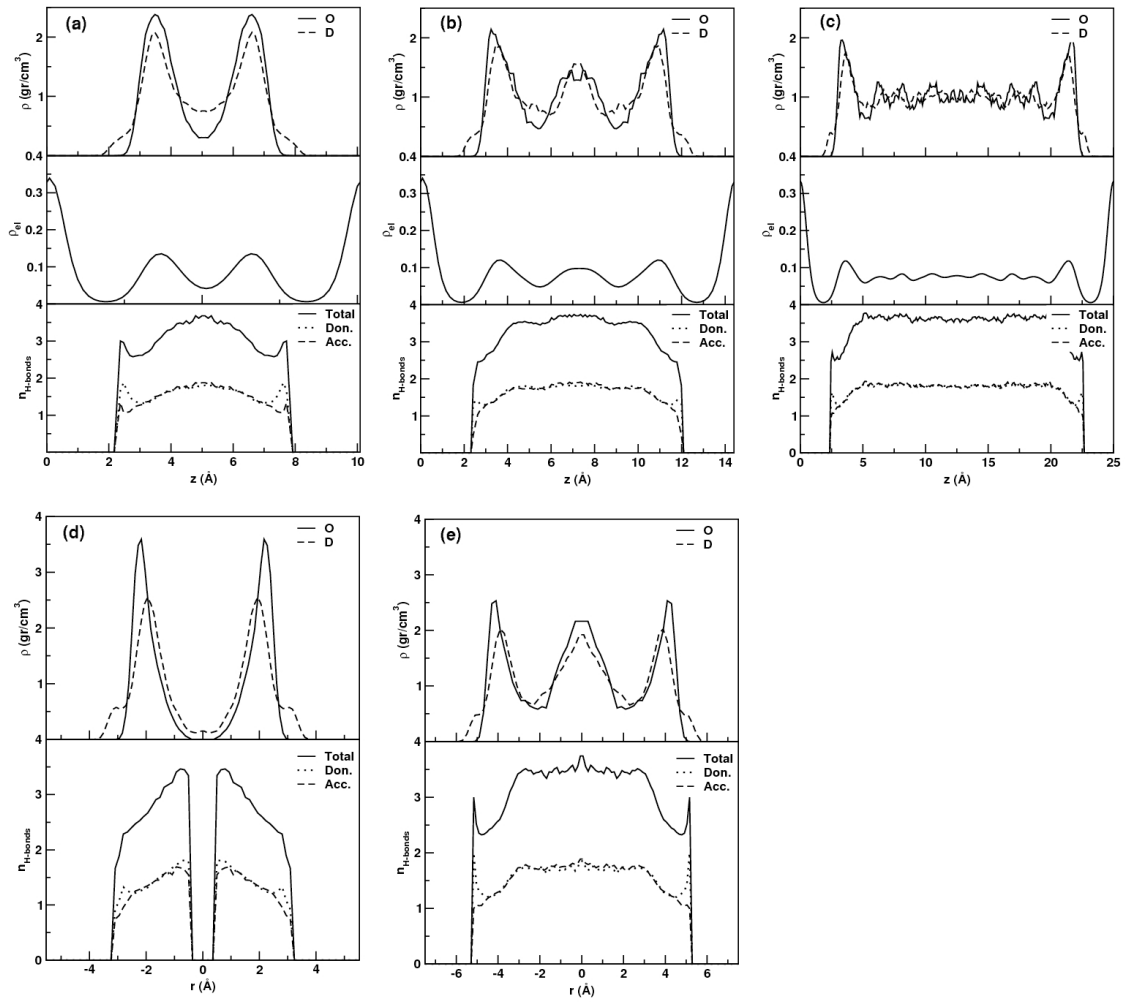

Figure 1. The top panels of a), b) and c) show the density of water molecules computed along the direction perpendicular to graphene confining surfaces (the continuous and dashed curves represent oxygen and deuterium atoms, respectively) for three confining lengths [a), 10.09 Å; b), 14.41 Å and c) 25.02 Å; see text]. The middle and bottom panels show the valence electronic charge density and the average number of water-water hydrogen bonds, respectively, corresponding to the three confining lengths. The curves in the bottom panels display the number of H-bond donor (dotted line) and acceptor (dashed line) for each water molecule; the total number of hydrogen bonds per molecule is also reported as a continuous black line. We choose the following geometric criterion to define a hydrogen bond:

O···O distance shorter than 3.5 Å and O···HO angle larger than 140º. The top and bottom panels of d) and e) show the water density and number of hydrogen bonds in the case of carbon nanotubes with diameter of 11.10 and 15.00 Å, respectively.

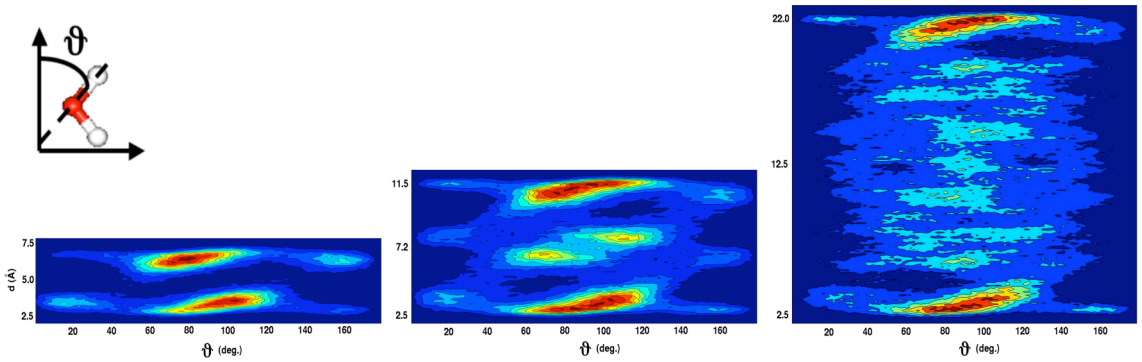

Figure 2. Tilt angle distribution for water molecules confined within graphene sheets, for the three confining lengths defined in Fig. 1. The tilt angle is defined with respect to the direction perpendicular to the surface. See inset for the definition of the tilt angle.

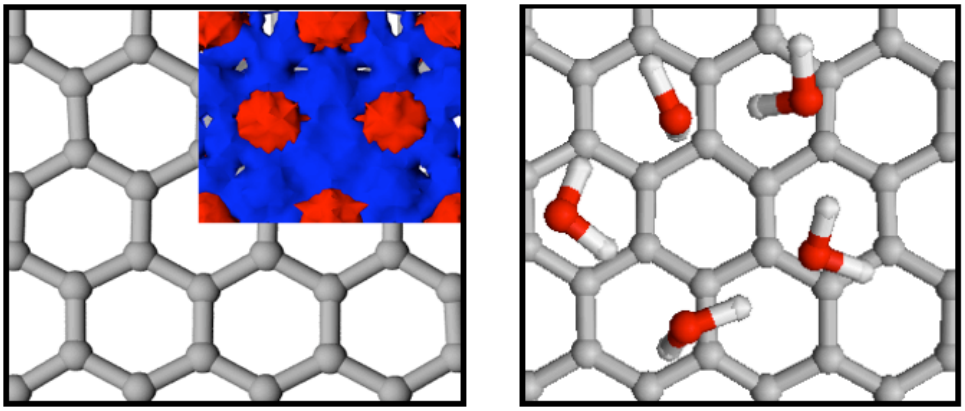

Figure 3. The left panel shows the oxygen (red isosurface) and deuterium (blue isosurface) spatial distribution function (SDF) of water molecules confined within graphene sheets at a distance of 14.41 Å (see also Fig.1b). These SDFs represent the density distribution of oxygen and deuterium atom positions in a layer within 5 Å from the graphene surface. The right panel contains a ball and stick representation of the water molecules at the interface for a representative snapshot of our MD trajectories. Red, white

and grey spheres represent oxygen, deuterium and carbon atoms, respectively. The restructuring of water close to the interface is responsible for the appearance of novel ring structures under confinement. In particular, the probability of finding 4-fold and 5-fold rings increases and that of finding 6-fold ones decreases, with respect to the bulk. [For a discussion of ring statistics around hydrophobic groups see, e.g. Ref. 64].

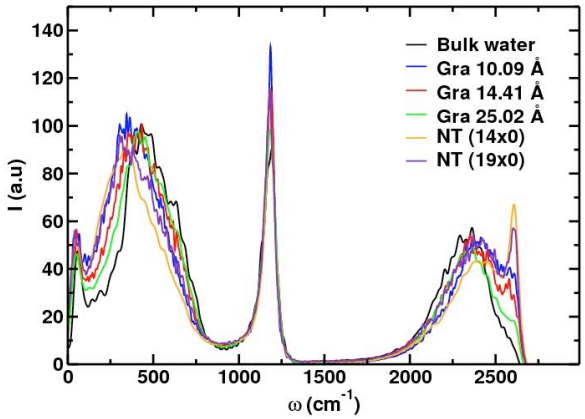

Figure 4. Comparison of the power spectra of the velocity-velocity autocorrelation function for all the confined water samples considered in this work. The power spectrum of bulk water is also reported for comparison.

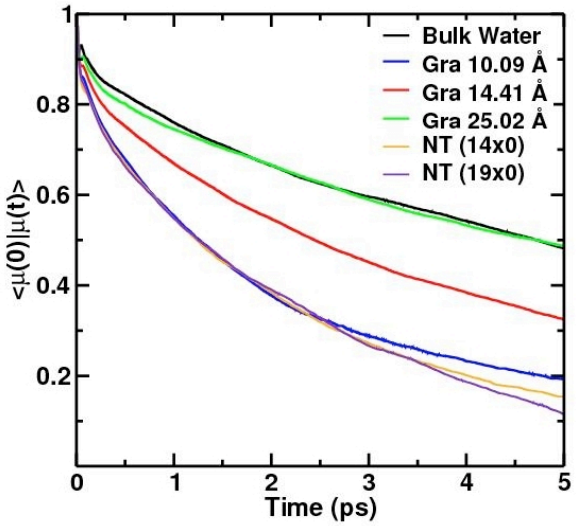

Figure 5. Water dipole rotational autocorrelation function for all the water samples considered here (see text), as obtained from *first principle* MD simulations. The relative dipole rotational autocorrelation functions of bulk water are also reported for comparison. Given the statistical error bars of our simulations (over ~ 20 ps runs), we can only make the observation that the autocorrelation functions for the 2.5 nm separation case is similar to the bulk case, but not exactly establish whether it has already reached the bulk value. It is instead clear that the correlation functions for smaller separations are decaying faster than in the bulk case (see text).

TABLES

System	d (Å)	N(D_2O)	t (ps)
Graphene	10.09	32	25
Graphene	14.41	54	20
Graphene	25.02	108	10
NT (14x0)	11.10	34	20
NT (19x0)	15.00	54	20

Table 1. For each simulation performed in this work, the confining length (d), the number of D_2O molecules (N) and the total simulation time t (ps) are given. In the case of graphene d represents the distance between the confining sheet, and in the case of nanotubes, it represents the diameter. All simulations are Born-Oppenheimer molecular dynamics simulations carried out using Density Functional Theory, with the PBE functional.

REFERENCES.

1. Hummer, G.; Rasaiah, J. C.; Noworyta, J. P. *Science* **2001**, *414*, 188.

2. Maibaum, L.; Chandler, D. *J. Phys. Chem. B* **2003**, *107*, 1189.

3. Beckstein, O; Sansom, M. S. P. *Proc. Nat'l Acad. Science* **2003**, *100*, 7063.

4. Holt, J. K.; Park, H. P.; Waang, Y.; Stadermann, M.; Artyukhin A-B.; Grigopoupulos, C. P.; Noy, A.; Bakajin, O. *Science* **2006**, *312*, 1034.

5. Majumder, M.; Chopra, N.; Andrews, R.; Hinds, B. J. *Nature* **2005**, *438*, 44.

6. Mashl, R-J.; Joseph, S.; Aluru, N-R.; Jakobsson, E. *Nano Lett.* **2003**, *3*, 589.

7. Koga, K.; Gao, G-T.; Tanaka, H.; Zeng, X. C. *Science* **2001**, *412*, 802.

8. Chandler, D. *Nature* **2005**, *437*, 640, and references therein.

9. Bellissent M.-C. *J. Mol. Liq.* **2002**, *96-97*, 287.

10. Cheng, L.; Fenter, P.; Nagy, K. L.; Schlegel, M. L.; Sturchio, N. C. *Phys. Rev. Lett.* **2001**, *87*, 156103.

11. Bagchi B. *Chem. Rev.* **2005**, *105*, 3197.

12. Naguib, N.; Ye, H.; Gogotsi, Y.; Yazicioglu, A. G.; Megaridis, C. M.; Yoshimura, M. *Nano Lett.* **2004**, *4*, 2237.

13. Major, R. C.; Houston, J. E.; McGrath, M. J.; Siepmann, J. I.; Zhu, X. Y. *Phys. Rev. Lett.* **2006**, *96*, 177803.

14. Raviv, U.; Laurat, P.; Klein, J. *Nature* **2001**, *413*, 51.

15. Raviv, U.; Klein, J. *Science* **2002**, 297, 1540.

16. Koga, K.; Gao, G. T.; Tanaka, H.; Zeng, X. C. *Physica A* **2002**, *314*, 462.

17. Kolesnikov, A. I.; Zanotti, J. M.; Loong, C. K.; Thiyagarajan, P.; Moravsky, A. P.; Loutfy R. O.; Burham, C. J. *Phys. Rev. Lett.* **2004**, *93*, 035503.

18. Ghosh, S.; Ramanathan K. V.; Sood, A. K. *Europhys. Lett.* **2004**, *65*, 678.

19. Zangi, R.; Mark, A. E. *Phys Rev. Lett.* **2003**, *91*, 025502.

20. Zangi, R.; Mark, A. E. *J. Chem. Phys.* **2003**, *119*, 1694.

21. Hirunsit, P.; Balbuena, P. B. *J. Phys. Chem. C* **2007**, *111*, 1709.

22. Rahman, A.; Stillinger, F. H. *J. Chem. Phys.* **1971**, *55*, 3336.

23. Jorgensen, W. L.; Chandrasekhar, J.; Madura, J. *J. Chem. Phys.* **1983**, 79, 926.

24. Martì, J.; Gordillo, M. C. *Chem. Phys. Lett.* **2000**, *329*, 341.

25. Martì, J.; Gordillo, M. C. *Phys. Rev. E* **2000**, *64*, 021504.

26. Martì, J.; Gordillo, M. C. *Phys. Rev. B* **2001**, *63*, 165430.

27. Gordillo, M. C.; Nagy, G.; Martì, J. *J. Chem. Phys.* **2005**, *123*, 054707.

28. Martì, J.; Nagy, G.; Gordillo, M. C.; Guardia, E. *J. Chem. Phys.* **2006**, *124*, 094703.

29. Liu, Y.; Wang, Q.; Wu, T.; Zhang, L. *J. Chem. Phys.* **2005**, *123*, 234701.

30. Liu, Y.; Wang, Q. *Phys. Rev. B* **2005**, *72*, 085420.

31. Hanasaki, I.; Nakatani, A. *J. Chem. Phys.* **2006**, *124*, 174714.

32. Choudhury, N.; Pettitt, B. M. *J. Phys. Chem. B* **2005**, *109*, 6422.

33. Pertsin, A. ; Grunze, M. *J. Phys. Chem B* **2004**, *108*, 1357.

34. Berendsen, J. C.; Grigera, J. R.; Straatsma, T. P. *J. Phys. Chem.* **1987**, *91*, 6269.

35. Werder, T.; Walther, J. H.; Jaffe R. L.; Halicioglu, T.; Noca, F.; Koumoutsakos, P. *Nano Lett.* **2001**, *1*, 697.

36. Hohenberg, P.; Kohn, W. *Phys. Rev.* **1964**, *136*, B864.

37. Kohn, W.; Sham, L. J. *Phys. Rev.* **1965**, *140*, A1133.

38. Perdew, J. P.; Burke, K. ; Ernzerhof, M. *Phys. Rev. Lett.* **1996**, *77*, 3865.

39. Hamann, D. *Phys. Rev. B* **1989**, *40*, 2980.

40. Grossman, J. C.; Schwegler, E.; Gygi, F.; Galli, G. *J. Chem. Phys.* **2004**, *120*, 300.

41. Schwegler, E.; Grossman, J. C.; Gygi, F.; Galli, G. *J. Chem. Phys.* **2004**, *121*, 5400.

42. Allesch, M.; Schwegler, E.; Galli, G. *J. Phys. Chem. B* **2007**, *111*, 1081.

43. Chen, B.; Ivanov, I.; Klein, M. L.; Parrinello M. *Phys. Rev. Lett.* **2003**, *91*, 215503.

44. Wang, C. Z.; Chan C. T.; Ho K. M. *Phys Rev. B* **1990**, *42*, 11276.

45. Porter, L. J.; Li J., Yip S. *Nucl. Mater.* **1997**, *246*, 53.

46. M. Sharma, *private communication.*

47. Birkett, G. R.; Do, D. D. *J. Phys. Chem. C* **2007**, *111*, 5735.

48. A general purpose *first principle* Molecular Dynamics code, F. Gygi, 1998-2007 (UCD).

49. A *first principle* Molecular Dynamics code, F.Gygi, 1998-2003 (LLNL).

50. Gygi, F.; Fattebert J. L.; Schwegler, E. *Comput. Phys. Commun.* **2003**, *155*, 1.

51. See: www.gromacs.org

52. Lee, S. H.; Rossky, P. J. *J. Chem. Phys.* **1994**, *100*, 3334.

53. Lee, C. Y.; McCammon J. A.; Rossky P. J. *J. Chem. Phys.* **1984**, *80*, 4448.

54. Poyron, A.; Hong, L.; Robinsin, I. K.; Granick S.; Zhang, Z.; P. A. Fenter *Phys. Rev. Lett.* **2006**, *97*, 266101.

55. Du, Q.; Freysz, Y.; Shen Y. R. *Science* **1994**, *264*, 826.

56. Cicero, G.; Grossman, J. C.; Catellani, A.; Galli, G. *J. Am. Chem. Soc.* **2005**, *127*, 6830.

57. Marzari, N.; Vanderbilt, D. *Phys. Rev. B* **1997**, *56*, 12847.

58. Scodinu, A.; Fourkas, J. T. J. *Chem. Phys. B* **2002**, *106*, 10292.

59. Kim, H. I.; Kushmmerick, J. G.; Houston, J. E.; Bunker, B. C. *Langmuir* **2003**, *19*, 9271.

60. Coudert, F. X.; Vuilleumier, R.; Boutin, A. *Chem. Phys. Chem.* **2006**, *7*, 2464.

61. Byl, O.; Liu, J. C.; Wang, Y.; Yim, W. L.; Johnson, J. K.; Yates, J. T. *J. Am. Chem. Soc.* **2006**, *128*, 12090.

62. Leng, Y.; Cummings, P. T. *Phys. Rev. Lett.* **2005**, 94, 026101.

63. Kumar, P.; Starr, F. W.; Buldyrev, S. V.; Stanley, H. E. *Phys. Rev. E.* **2007**, *75*, 011202.

64. Head-Gordon, T. *Proc. Nat'l. Acad. Soc.* **1995**, *92*, 8308.

TOC grafic: